Jalayer, F., Carozza, S., De Risi, R., Manfredi, G., & Mbuya, E. (2016). Performance-based flood safety-checking for non-engineered masonry structures. *Engineering Structures*, *106*, 109-123. https://doi.org/10.1016/j.engstruct.2015.10.007

Performance-based flood safety-checking for non-engineered masonry structures

Fatemeh Jalayer[1], Stefano Carozza*[1], Raffaele De Risi[1,1], Gaetano Manfredi[1], Elinorata Mbuya[2]
[1]Deptartment of Structures for Engineering and Architecture, University of Naples Federico II, Italy
[2]Institute of Human Settlements Studies (IHSS), Ardhi University, Dar es Salaam, Tanzania
*Corresponding author: stefano.carozza@unina.it

Abstract

Demand and Capacity Factor Design (DCFD) is a probability-based safety-checking format for performance-based seismic design and assessment of structures. Inspired from the original DCFD formulation for seismic excitation, this work proposes a similar performance-based safety-checking format for flooding, adopting the flood height as the intensity measure. The proposed DCFD formulation implements the fragility/hazard parameters for flooding. The structural fragility is evaluated by adopting an efficient and simulation-based method yielding the so-called "robust" fragility curve and an associated plus/minus one-standard deviation interval. The structural performance is measured by the (critical) demand to capacity ratio for the weakest element of the weakest wall within the structure, subjected to a combination of hydro-static, hydro-dynamic and accidental debris impact loads. Analogous to the incremental dynamic analysis method proposed for seismic demand assessment, an incremental flood height analysis is used to monitor the structural performance as a function of increasing water height. For each structural modelling configuration, generated based on the characterization of uncertainties in loading and material mechanical properties, the incremental flood height analysis is employed in order to calculate the critical water height corresponding to a demand to capacity ratio of unity. The application of the proposed methodology is demonstrated for both flood fragility/risk assessment and comparative screening of various viable flood mitigation strategies for a non-engineered building made of cement bricks in Dar Es Salaam, Africa.

Key Words

Hydro-geological hazards; Flood risk assessment; Upgrade decision-making; Structural vulnerability; Informal settlements.

Introduction

Non-engineered structures can be characterized by un-classified construction practice, non-well-documented material mechanical properties, lack of reference technical codes and lack of a structural design basis. Aforementioned qualities would arguably result in buildings that are particularly vulnerable to extreme natural events. As far as it regards hydro-geological hazards like flooding, this very often pairs up with poor and un-informed "choice" of the construction site. Considering their un-programmed nature, the non-engineered building sites often coincide with flood plains and potentially flood-prone areas.

Flooding vulnerability and risk assessment is the subject of increasing attention in the past decades. Smith and Greenway [1], Torres et al. [2], Davis [3], Scawthorn et al. [4, 5] define general methodological approaches to flood risk assessment. Various research efforts are focused on several aspects of flooding problem, such as loss of life [6, 7], economic losses [8, 9], and damage to

[1] Currently a Research Assistant at Bristol University: raffaele.derisi@bristol.ac.uk

buildings [10-12]. These works are mainly based on damage observed after the flooding event classified using different discrete scales. Kelman [13] classifies the damage with a scale of six damage states (from DS0 to DS5) from no water contact to structural collapse or undermining of the foundation. Analogous to the definition of the damage grades in the European Macroseismic Scale EMS-98 [14], Schwarz and Maiwald [11, 15] proposed a modified damage scale distinguishing between structural and non-structural damage. Charvet et al. [16] have applied a statistical model to assess the fragility of different buildings to Tsunami based on the damage state classification of the Ministry of Land, Infrastructure and Transport (MLIT) index damage state (DS) after the tsunami occurred in Japan (2011). Formulations to assess the vulnerability of a building in terms of damage state probability are proposed by Haugen and Kaynia [17] (for the impact of debris flow) and Nadal et al. [18] (for riverine and coastal floods). Dawson et al. [19] have evaluated the flooding risk of a dike system through a sampling technique in a MC simulation approach. Yue and Elligwood [20] have highlighted the importance of considering the modelling uncertainties in the assessment of hurricane risk for different configurations of structures (e.g. different number of floors, connection systems, materials). Very few analytical models for vulnerability assessment have so far been proposed for flash-flood and debris flow phenomena. Nigro and Faella [21] have classified the various resisting mechanisms for reinforced concrete frames and masonry structures. They have used limit analysis in order to calculate the critical flow velocity that can activate a mechanism in the structure. Haugen and Kaynia [17] have proposed a methodology for calculating the dynamic response of an equivalent single degree of freedom system to debris flow impact.

This work documents the research being conducted in the context of the European FP7 project Climate Change and Urban Vulnerability in Africa (CLUVA) with regard to flooding vulnerability of informal settlements. In previous works, De Risi et al. [22], Jalayer et al. [23] and [24], De Risi et al. [25] and [26], the authors have proposed two distinct approaches for flood risk assessment for urban areas in Africa suitable for micro- and meso-scale, respectively. The work by De Risi et al. [22], which focuses on flood risk assessment in micro-scale, illustrates how a modular performance-based methodology for risk assessment (a.k.a, the Pacific Earthquake Engineering Research (PEER) approach for seismic risk assessment; see for example, Cornell et al. [27]) can be used in order to calculate the flooding risk for a portfolio of informal settlements. Along the same lines and focusing on the assessment of structural vulnerability, the present work applies the Demand and Capacity Factor Design (DCFD) for safety-checking and upgrade decision-making for informal settlements. The original DCFD is a probability-based safety-checking format for seismic assessment (Cornell et al. [28] and Jalayer and Cornell [29]). According to this format, the factored capacity is compared with the factored demand corresponding to a prescribed allowable risk [29]. Using the flooding height as the intensity measure between hazard and fragility, the structural capacity for a prescribed limit state is described in terms of the critical water height corresponding to the limit state in question. In the context of safety-checking based on DCFD format, this translates into comparing the factored critical flood height for a given building to the flooding height corresponding to a prescribed return period, providing an efficient and graphical procedure for structural assessment and upgrade decision-making [30].

1 Methodology

1.1 Limit states, the performance variable and the sources of uncertainty

The structural limit states are used as a proxy in order to describe the various damage states in the structure. This paper focuses on the limit state of collapse (CO) that is identified based on the corresponding critical water height threshold. This choice is further justified recalling that the flood height can be used as the scalar intensity measure for the integration of flooding hazard and

vulnerability to calculate the flood risk [22]. The structural collapse limit state consists in the failure of the bearing structure, collapse of the walls, loss of support of the roof, or loss of loading bearing capacity of the building due to elongated contact with water or deterioration. Generally speaking, structural collapse entails the loss of vertical loading capacity in the structure. The structural limit state exceedance is described herein in terms of a structural *performance variable* --denoted as Y and defined in terms of a systemic critical demand to capacity ratio-- that exceeds unity for the limit state in question. Given the potential fragile nature of collapse and the possible lack of box behaviour in non-engineered buildings, it has been chosen to define the critical demand to capacity ratio according to a *weakest link* formulation where the weakest element in the structure arrives to the onset of collapse limit state [31].

As it has been mentioned above, the flooding height is being used as the *intensity measure;* that is, the parameter in terms of which the evaluation of capacity and demand is performed. Consequently, it has been chosen to work with a structural performance variable defined as the critical flooding height corresponding to Y=1; where Y is the critical demand to capacity ratio defined in the previous paragraph. This structural performance variable is denoted generically as $h_{Y=1}$. In fact, the use of limit state thresholds defined in terms of the intensity measure is already established and examples can be found in various works such as [32, 33]. Based on the definitions presented herein, the flooding fragility, defined as the probability of exceeding the limit state conditioned on the flooding height h can be described as:

$$P(LS \mid h) = P(Y > 1 \mid h) = P(h_{Y=1}(\boldsymbol{\theta}) < h) \quad \text{Eq. 1}$$

It should be noted that the critical water height $h_{Y=1}$ is a function of the uncertain parameters $\boldsymbol{\theta}$ present in the fragility estimation problem. However, for the sake of brevity, the dependence on $\boldsymbol{\theta}$ is dropped hereafter. The structural fragility can also be interpreted as the cumulative distribution function for the performance variable or critical water height $h_{Y=1}$. In general, the uncertainties in the vulnerability assessment of non-engineered structures can be classified in three main categories, namely, (a) the uncertainties in the characterization of material mechanical properties; (b) the uncertainties in the characterization of the structural and geometrical modelling parameters; and (c) the uncertainties in loading. In the case-study presented in this work only the uncertainties in mechanical material properties and loading (only related to debris impact) are considered.

1.2 The Incremental Flood Height Analysis (IFHA)

For a given realization of the vector of uncertain parameters $\boldsymbol{\theta}$, the incremental flood height analysis procedure consists of calculating the value of the critical demand to capacity ratio in the structure for increasing values of flooding height. That is, for each given value of the water height h, the critical demand to capacity ratio Y is calculated for the structure and the resulting Y-h data points can be connected in order to form the incremental flood height analysis (IFHA) curve. Figure 1 shows a schematic representation of an IFHA curve.

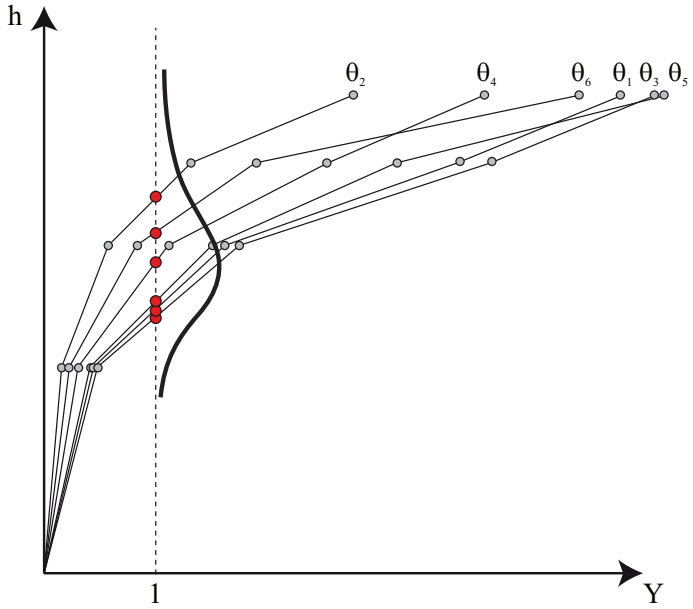

Figure 1: Typical incremental flood height analysis curves.

It can be noted that a given IFHA curve corresponds to a prescribed realization of the vector of parameters θ. Therefore, a sample of θ vector realizations would lead to sample of IFHA curves. It can also be noted that the IFHA curve can be used to find (by interpolation) the critical water height value corresponding to the onset of (a prescribed) limit state identified as Y=1.

1.3 An Efficient Bayesian fragility assessment procedure

Jalayer et al. [34, 35] have discussed how a simulation-based Bayesian procedure can be employed in order to derive flooding fragility curves conditioned on a Log Normal fragility model. This method can efficiently implement the results of the incremental flood height analysis (i.e., the critical flooding height values corresponding to Y=1) for a limited sample of θ realizations as "*data*" in order to provide a *robust* flood fragility curve (as a mean estimate over all possible fragility curves defined by a prescribed model, e.g., Log Normal model) and the mean plus/minus one standard deviation curves. In this section, a brief overview of this method is provided.

Suppose that a Log Normal distribution identified by the vector of parameters $\chi=[\eta, \beta]$ has been chosen as the underlying fragility model[2]:

$$F\left(LS \mid h, \chi\right) = P\left(h_{Y=1} \le h \mid \eta, \beta\right) = \Phi\left(\frac{\ln(h/\eta)}{\beta}\right) \qquad \text{Eq. 2}$$

where the parameters $\chi=[\eta, \beta]$ stand for the median and the logarithmic standard deviation for the distribution of the natural logarithm of the critical flood height value corresponding to the onset of limit state denoted by $h_{Y=1}$. The joint probability distribution for parameters χ of the Log Normal distribution given vector ***D*** (e.g., the vector of critical flood height values calculated from the *IFHA*

[2] The lognormal model is perhaps the most universally adopted model for structural fragility. Three factors may have contributed to this ubiquitous use; namely, the simplicity, non-negative argument variable, and the fact that it relies only on the first two (non-central) statistical moments (i.e., mean and standard deviation). Arguably, in circumstances where only the first two statistical moments are available, the Normal (Log Normal) distribution is an optimal probability distribution to adopt ([36] Jaynes ET. Probability theory: the logic of science: Cambridge university press; 2003.). It is worth mentioning that using a Log Normal fragility model usually leads to more accurate estimations for the central part of the distribution. In other words, the Log Normal fragility model might not be the most suitable choice for tail-sensitive data.

curves) can be expressed as the posterior joint probability distribution for the mean and standard deviation for the Normal probability distribution [37]:

$$p(\chi \mid \mathbf{D}) = p(\eta, \beta \mid \mathbf{D}) = p(\eta \mid \beta, \mathbf{D}) \cdot p(\beta \mid \mathbf{D}) \quad \text{Eq. 3}$$

where $p(\beta|\boldsymbol{D})$ is the posterior marginal distribution of β and $p(\eta|\beta,\boldsymbol{D})$ is the posterior conditional distribution of η given β. The marginal PDF for β can be expressed as a derived χ distribution [37]:

$$p(\beta \mid \mathbf{D}) = \left[\frac{1}{2} \cdot \Gamma\left(\frac{n}{2}\right)\right]^{-1} \cdot \left(\frac{\upsilon \cdot s^2}{2}\right)^{\frac{n}{2}} \cdot \beta^{-(n+1)} \cdot e^{-\frac{\upsilon \cdot s^2}{2 \cdot \beta^2}} \quad \text{Eq. 4}$$

The posterior conditional distribution of η can be calculated as [37]:

$$p(\eta \mid \beta, \mathbf{D}) = \sqrt{\frac{N}{2 \cdot \pi \cdot \beta^2}} \cdot e^{-\frac{N \cdot \left(\ln \eta - \overline{\ln h_{Y=1}}\right)^2}{2 \cdot \beta^2}} \quad \text{Eq. 5}$$

where ν=N-1; $\overline{\ln h_{Y=1}}$ and s^2 are the (logarithmic) sample average and sample variance of the set of structural performance variable values $h_{Y=1}$ for limit state *LS*, respectively. Finally, the *robust fragility* can be calculated by integrating over the joint (posterior) probability distribution for the Log-Normal fragility model conditioned on the set of data values obtained in the form of $D = \{D_i = h_{i,Y=1}\}$

$$P(LS \mid h, \mathbf{D}) = E_{\chi}[F(LS \mid h, \mathbf{D}, \chi)] = \int_{\Omega(\boldsymbol{\chi})} \Phi\left(\frac{\ln(h/\eta)}{\beta}\right) \cdot p(\boldsymbol{\chi} \mid \mathbf{D}) \cdot d\boldsymbol{\chi} \quad \text{Eq. 6}$$

where $E_{\chi}[.]$ is the expected value operator over the vector of parameters χ =[η, β] and $\boldsymbol{\Omega}$ is the domain of vector χ. The variance σ^2 in fragility estimation can be calculated as:

$$\sigma_{\chi}^2 F = E_{\chi}[F(LS \mid h, \mathbf{D}, \chi) - P(LS \mid h, \mathbf{D})]^2 = \int_{\Omega(\boldsymbol{\chi})} [\Phi\left(\frac{\ln(h/\eta)}{\beta}\right) - P(LS \mid h, \mathbf{D})]^2 \cdot p(\boldsymbol{\chi} \mid \mathbf{D}) \cdot d\boldsymbol{\chi} \quad \text{Eq. 7}$$

where $P(LS|h, \boldsymbol{D})$ is calculated from Eq. 6.

1.3.1 Calculation of robust fragility using Monte Carlo Simulation

The robust fragility curve and its plus/minus one standard deviation confidence interval can be calculated efficiently using Monte Carlo Simulation. This is done by approximating Eq. 6 and Eq. 7 in the following manner:

$$P(LS \mid h, \mathbf{D}) \approx \tilde{R} = \frac{\sum_{i=1}^{n_{sim}} \Phi\left(\frac{\ln(h/\eta_i)}{\beta_i}\right)}{n_{sim}} \quad \text{Eq. 8}$$

and,

$$\sigma_{\chi}^2 F \approx \frac{\sum_{j=1}^{n_{sim}} \left[\Phi\left(\frac{\ln(h/\eta_j)}{\beta_j}\right) - \tilde{R}\right]^2}{n_{sim}} \quad \text{Eq. 9}$$

Where n_{sim} is the number of simulations. In above equations, η_i and β_i correspond to the i^{th} realization of the vector of fragility parameters χ_i. The vector χ_i is simulated based on its probability density function $p(\chi|\boldsymbol{D})$ in Eq. 3. This is achieved by first sampling β_i from its (posterior) marginal probability distribution $p(\beta|\boldsymbol{D})$ in Eq. 4. In the next step, conditioning on β_i, η_i is sampled form the conditional (posterior) distribution $p(\eta|\beta_i, \boldsymbol{D})$ in Eq. 5. It should be noted that n_{sim} can assume very

large values with no problem as the estimators shown in Eq. 8 and Eq. 9 and the probability distributions in Eq. 4 and Eq. 5 are all expressed in a closed and analytic from.

1.4 Implementing IFHA in a performance-based safety-checking framework

A performance-based safety-checking objective can be expressed by the following generic inequality:

$$\lambda_{LS} \le \lambda_o \qquad \text{Eq. 10}$$

where λ_{LS} is the mean annual frequency of exceeding a prescribed limit state (i.e., a proxy for flooding risk) and λ_{LS} is an acceptable risk level, expressed in terms of the annual frequency of exceedance or one over the return period T_R. The robust flooding fragility curve denoted as $P(LS|h,\boldsymbol{D})$ (calculated in the previous section) can be integrated with flooding hazard $\lambda(h)$, expressed in terms of the mean annual frequency of exceeding a certain flooding height h, in order to calculate the mean annual frequency of exceeding a prescribed limit state λ_{LS} in a specific point within the basin [22].

$$\lambda_{LS} = \int_{\Omega_h} P(LS \mid h,\mathbf{D}) \left| d\lambda(h) \right| \qquad \text{Eq. 11}$$

1.4.1 IFHA in Demand and Capacity Factor Design (DCFD)

The mean annual frequency of exceeding a prescribed limit state (risk) λ_{LS} can be expressed in a simple closed-form and analytical formulation based on the following set of simplifying assumptions [28, 38]: the robust fragility $P(LS|h,\boldsymbol{D})$ can be expressed as a Log Normal cumulative distribution function (CDF) with median $\eta_{h(Y=1)}$ and logarithmic standard deviation $\beta_{h(Y=1)}$; the flooding hazard curve can be approximated by a power-law relation as a function of the flooding height $k_o \cdot h^{-k}$. As a result, the performance objective in Eq. 10 can be expressed as following:

$$\lambda_{LS} = k_o \cdot \left(\eta_{h_{Y=1}}\right)^{-k} \cdot \exp\left(\frac{1}{2} k^2 \cdot \beta^2{}_{h_{Y=1}}\right) \le \lambda_o \qquad \text{Eq. 12}$$

After simple algebraic manipulations, Eq. 12 can be rearranged and subsequently expressed as:

$$\left(\frac{\lambda_o}{k_o}\right)^{\frac{-1}{k}} \le \eta_{h_{Y=1}} \cdot \exp\left(-\frac{1}{2} k \cdot \beta^2{}_{h_{Y=1}}\right) \qquad \text{Eq. 13}$$

The above performance-based safety-checking inequality can be represented in the following generic format:

$$h(T_R) \le FC \qquad \text{Eq. 14}$$

where $h(T_R)$ is the flooding height corresponding to the flooding return period $T_R=1/\lambda_o$ from the flood hazard curve or simply *"flood demand"*; FC is referred to as the factored critical flooding height or simply *"factored capacity"* (e.g., in meters of water height):

$$FC = \eta_{h_{Y=1}} \cdot \exp\left(-\frac{1}{2} k \cdot \beta^2{}_{h_{Y=1}}\right)$$
$$h(T_R) = \left(\frac{\lambda_o}{k_o}\right)^{\frac{-1}{k}} \qquad \text{Eq. 15}$$

In the presence of epistemic uncertainties for determining the median flooding height, it can be shown [28] that the factored capacity FC_U can be calculated from the following:

$$FC_U = \eta_{h_{Y=1}} \cdot \exp\left(-\frac{1}{2} k \cdot \beta^2{}_{h_{Y=1}}\right) \cdot \exp\left(-\frac{1}{2} k \cdot \beta^2{}_U\right) \qquad \text{Eq. 16}$$

where β_U represents the epistemic uncertainties in the estimation of the median flooding height from the fragility curve (i.e., the uncertainty in the parameters of the fragility model).

Figure 2 below shows a schematic representation of the factored capacity FC and the flood demand $h(T_R)$. The figure features both the robust fragility curve (solid blue line) and its plus/minus one standard deviation curves (dashed blue lines). The flooding hazard curve is plotted as a red solid line. As it can be seen from the figure, $\beta_{h(Y=1)}$ is estimated as half of the logarithmic distance between the 84th and 16th percentiles. The factored capacity FC calculated from Eq. 15 is shown as a full blue dot on the Figure. Moreover, estimating the epistemic uncertainty β_U as half of the logarithmic distance between the robust fragility plus and minus one standard deviation curves, the factored capacity FC_U is calculated taking into account the influence of the epistemic uncertainties (shown as the red full dot). This graphical representation is used later on for both the safety-checking of the default non-engineered structure of the case-study and also for upgrade decision-making for various viable mitigation strategies.

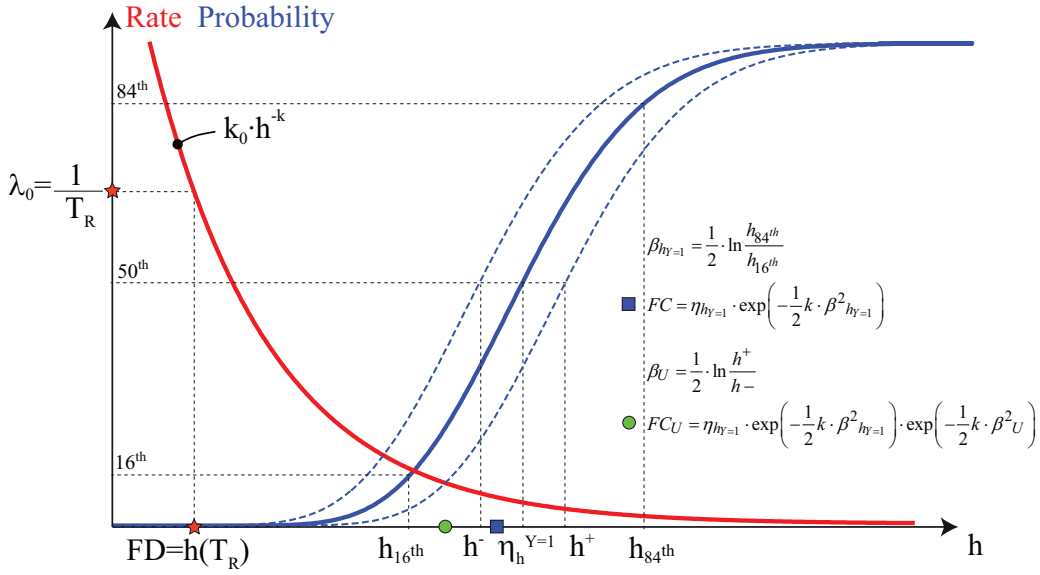

Figure 2: The schematic diagram of the DCFD safety checking format.

1.5 Flood actions

In this work, the structural damage induced by flooding is assumed to be due to hydrostatic and/or hydrodynamic pressure, and the accidental action induced by the impact of waterborne debris [39].

The hydro-static pressure: The hydro-static pressure $p_{hs}(z)$ is governed by Stevin's law, and can be calculated trough the following relation:

$$p_{hs}(z) = \gamma_w \cdot (h - z) \qquad \text{Eq. 17}$$

where γ_w is the specific weight of water, z is the abscissa measured from the bottom of the structure and h is the flooding height. It should be noted that the special case in which the foundation is under the ground level is not considered; in that case, hydrostatic pressure due to the soil column should also be considered.

The hydro-dynamic pressure: The hydrodynamic actions can be induced due to both flow velocity and also due to transient water level (i.e., waves). However, in an urban context, the hydrodynamic actions due to velocity of the flow seem to be more critical, as also shown in [40]. The hydro-dynamic pressure p_{hd} at height z from the ground can be derived as:

$$p_{hd}(z) = C_d \cdot \rho_w \cdot v^2(z)$$ Eq. 18

where C_d is the drag coefficient (typically ranges between 1.2 and 2.0 according to [41]); ρ_w is the mass density of the water ($\rho_w = \gamma_w / g$, with g gravity acceleration); $v(z)$ is the flow velocity at height z. It can be observed that the hydrodynamic pressure distribution is directly related to the velocity profile along the height. In lieu of detailed hydraulic calculations, the distribution of velocity along the height can be obtained based on simplified assumptions. Figure 3 below illustrates a typical representation of the velocity profile along a vertical surface. It can be observed that the maximum velocity is reached somewhat below the water surface.

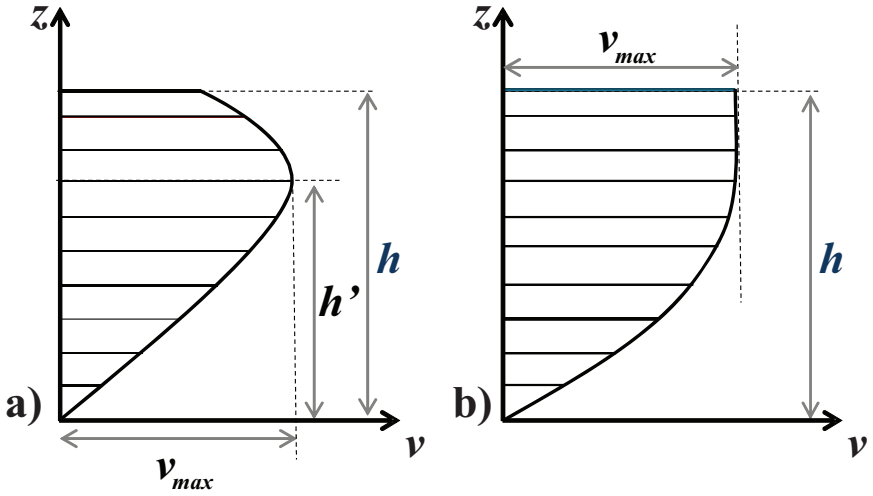

Figure 3: (a) Velocity profile along the height. (b) Approximate velocity profile.

In this work, an approximate velocity profile along the structural height is assumed as illustrated in Figure 3(b). This consists in adopting a parabolic profile that reaches the maximum velocity at the flow surface with a vertical slope. The approximate parabolic profile can be written as a function of the flooding height:

$$\frac{v(z)}{v_{max}} = -\left(\frac{z}{h}\right)^2 + 2 \cdot \left(\frac{z}{h}\right)$$ Eq. 19

As shown in [22, 42], the relation between maximum flooding velocity and maximum flooding height at any given point within the zone of interest can be approximated with a power-law relation (of the form $v_{max} = a \cdot h_{max}^{\ b}$). This power-law fit helps in transforming an otherwise vector-based risk assessment using $\mathbf{H} = [h_{max}, v_{max}]$ as the hazard/fragility intensity measure to a scalar risk assessment problem using only h_{max} as the intensity measure. The assumption that the maximum flow velocity versus maximum depth can be described by a power-law relation, in the context of this work, implies the following: 1) the maximum flow velocity occurs at the water surface level (it usually occurs somewhat below the water surface); 2) the maxima in velocity and depth take place simultaneously; 3) in a conservative manner, it has been assumed that the flow direction is orthogonal to the wall(s). It has been demonstrated in [22] that the flow velocity and depth maxima for various return periods indeed follow a power-law relation for the same neighbourhood of the case-study building herein. The median and logarithmic standard deviation for a and b parameters calculated for the Suna neighbourhood are [2.31, 0.13] and [1.77, 0.54], respectively.

The flood pressure profile: The flood pressure profile is calculated as the sum of the hydrostatic and hydrodynamic pressure profiles, at a given height from the ground level. Figure 4 below illustrates the total pressure acting on the wall panel (the right-hand column) and its break-down into hydro-static and hydro-dynamic components for a set of increasing flooding heights and

for two alternative combinations of the pair of the power law parameters (denoted as *a* and *b)*, namely (0.3, 1.15) and (1.5, 1.15). These two pairs of values are representative of two points with low flood velocity and height, and high flood velocity and low flooding height, respectively.

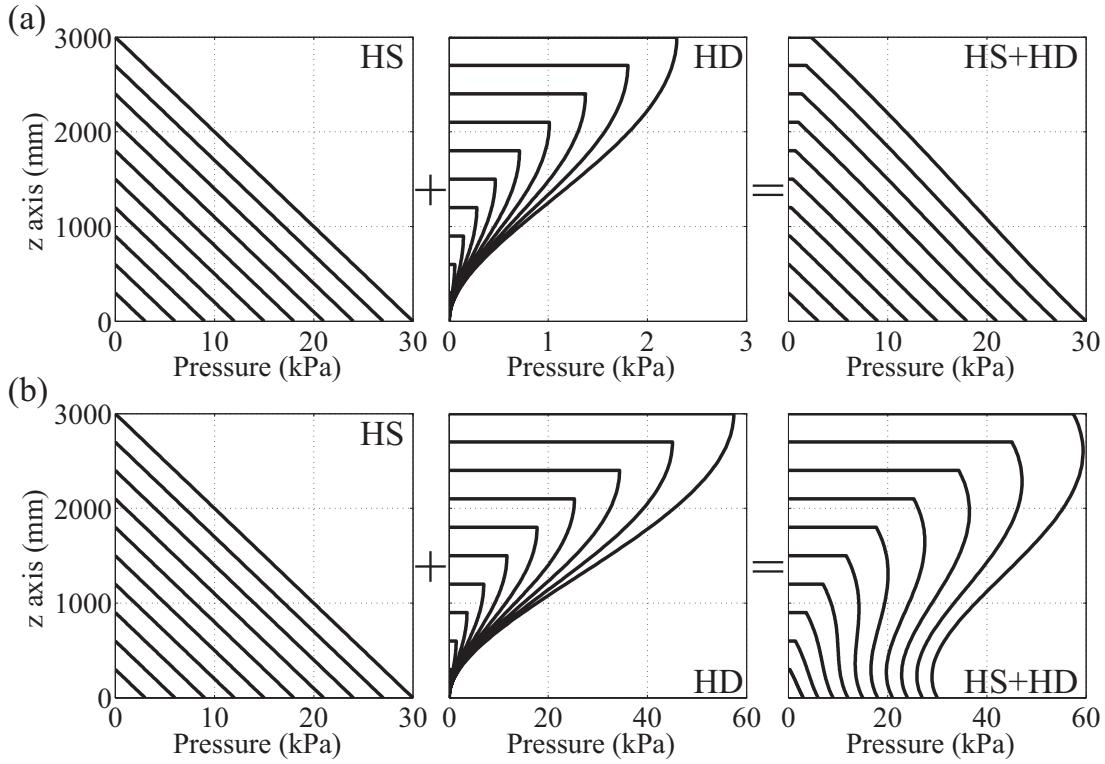

Figure 4: Break-down of the flood pressure profile into hydro-static and hydro-dynamic components for two different pairs of parameters (HS: hydrostatic; HD: hydrodynamic). (a) Low flooding height and low velocity. (b) Low flooding height and high velocity.

It can be observed that the contribution of hydro-dynamic pressure is significant for the case shown in Figure 4(b), with small flooding height and large flooding velocity. Generally speaking, the hydrodynamic pressure can be more significant for flood velocity values larger than 1 m/s.

Accidental debris impact: Once the velocity profile is known, it is possible to calculate the (accidental) debris impact forces. There are alternative formulations for the calculation of the impact magnitude leading to substantially equivalent results in the case of tree-trunk impact; for instance, the impulse-momentum [43], the work-energy [44] and the contact stiffness [45] formulations. The two latter approaches require information about the kind of debris that hit the structure. More specifically, the approach based on work-energy requires information about the stopping distance. This is while the approach based on contact stiffness needs to know the contact stiffness of the impact of the debris against the structure. Thus, in this work the approach outlined in [43] based on impulse-momentum formulation has been adopted to calculate the debris impact. The debris impact (F_{DI}) can be calculated through the following relation:

$$F_{DI} = \frac{W_D \cdot v_D}{g \cdot t} \qquad \text{Eq. 20}$$

where W_D is the debris weight; v_D is the debris velocity (assuming that the debris is waterborne, v_D=v_{max}); g is the gravity acceleration; and t is the impact duration.

Within the simulation procedure, the debris mass, the impact time and the horizontal position of the point of impact along the wall are going to be randomized.

2 Case study: cement block non-engineered buildings in Dar Es Salaam, Suna Neighbourhood

2.1 General description

Typical non-engineered residential buildings in Suna neighborhood in Dar Es Salaam are made of regular masonry with cement blocks [46, 47]. They may have a different percentage of hollow space and are not always placed with mortar layers. The walls are generally not protected with a waterproof layer. The thickness of wall is almost invariable and is generally equal to the thickness of the cement block (125mm) plus the plaster thickness (between 10-20 mm). A detailed survey conducted by the Institute of Human Settlements Studies (IHSS, Ardhi University) group on an informal building located in Suna neighborhood has been chosen as a representative case for cement brick non-engineered buildings in Dar Es Salaam [22]. The compiled survey sheet for this building is reported in the Appendix.

2.2 The structural model

This work employs an elastic finite element model (FEM) in the open-source software OpenSees [48]. Employing FEM provides the possibility of modelling the real geometry of the structure, taking into account the openings and irregularities. The structural models developed herein are consisted of two-dimensional elastic shell finite element panels with openings (considered as voids). Based on the detailed survey conducted on the case-study building, it is deducted that the vertical connections between the walls are not strong enough to activate a significant interaction between the orthogonal walls (a.k.a. box-effect). Therefore, the structure is modelled as an ensemble of individual 2D walls. Figure 5 and Figure 6 below illustrate the various configurations of the walls considered in the analysis procedure.

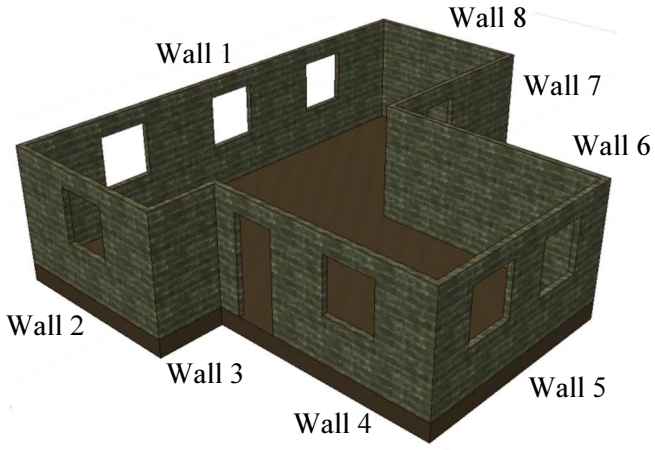

Figure 5: Three-dimensional view of the structural model.

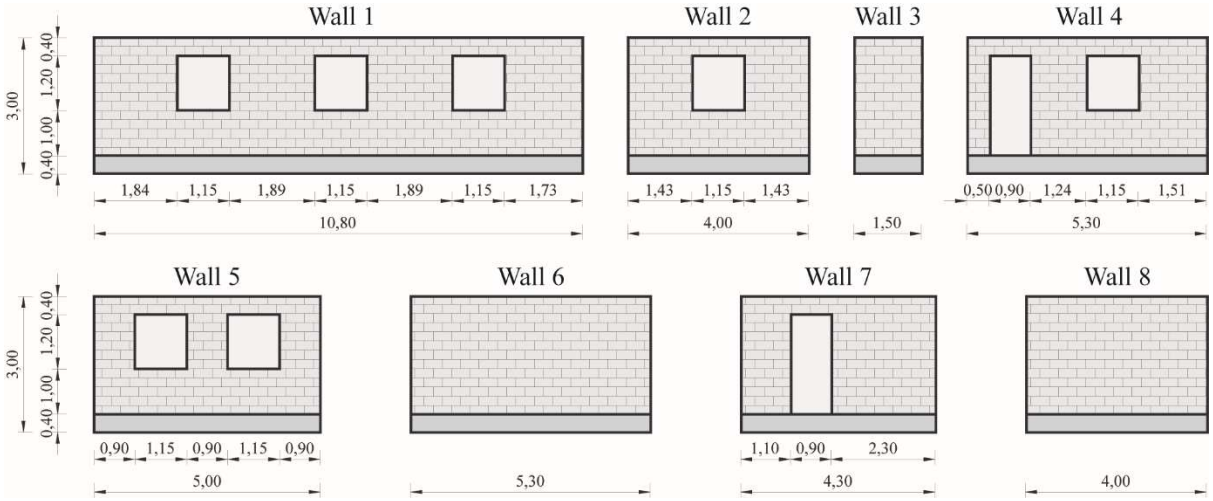

Figure 6: The individual two-dimensional wall panels modelled with OPENSEES (Length in meters).

It can be observed that the case-study building is composed of three completely full walls, three walls with only windows, one wall with door and window and one wall with only door. The rigidity of the connection between the walls is not known so that wall models may be considered hinged or fixed -end (clamped) at the vertical side. However, due to the absence of particular brick positioning details in the wall corners and the low thickness of the wall panel, the vertical wall constraint is assumed to be hinged. Since the building is realized on a raised platform of 40cm height, the bottom side of the wall is modeled as fixed (clamped). The platform consists of a plate foundation (under the entire building) raised from the ground in order to mitigate the problem of water entrance inside the building. The height of the platform is not subjected to uncertainty since it has been measured during the field survey.

2.3 Characterization of uncertainties

The mechanical material properties for this building are characterized by a considerable amount of uncertainty. This is due to both the variability of the material strength values in different parts of the same building (e.g., some parts of the structure may suffer degradation due to elongated and direct contact with water) and the lack of laboratory tests. To take into account these uncertainties, the mechanical properties of materials are characterized by probability distributions. In the following table, the material mechanical properties for the case-study building are reported.

Mechanical properties	Distribution type	Min	Max	COV [%]
γ (kN/m^3) – specific weight	Uniform	14.0	18.0	7.22
f_m (MPa) – compression strength	Uniform	1.0	3.0	28.87
τ_0 (MPa) – shear strength	Uniform	0.03	0.1	31.09
f_{fl} (MPa) – flexural strength	Uniform	0.12	0.15	6.42
E (MPa) – linear elastic modulus	Uniform	1200	1200	0.0

Table 1: Mechanical properties for Dar Es Salaam case study building.

The absence of a waterproof paint on the walls may reduce the mechanical properties of the material due to various factors, such as, direct contact with water, the presence of active agents and humidity. Since the building survey does not indicate whether the walls have water-proof paint or not, it is conservatively considered without water-proof protection. An overall reduction coefficient of 0.75 has been applied to all the material mechanical properties in order to take into account the

degrading material properties due to direct contact with environment [46]. However, it is worth mentioning that this value has been chosen in an arbitrary manner due to a complete lack of (quantitative) supporting information.

As mentioned in the previous section, the flood loading takes into account the effect of hydrostatic loading, hydrodynamic loading and the accidental debris impact. According to the survey sheet illustrated in Appendix, the doors and windows are not sufficiently water-proof. The effect of insufficient closure system is explicitly considered in calculating the flooding actions applied to the building. In particular, for this case study, hydrostatic load is not going to be considered in cases where the water level reaches the height of the platform. This is due to the fact that the presence of water inside the building leads to a distribution of hydrostatic pressure that equilibrates the external (hydrostatic) pressure.

The debris weight, duration of the debris impact and the point of impact within each wall have been assumed as the uncertain parameters governing the characterization of the debris impact. The first two have been considered uniformly distributed and their parameters are reported in Table 2 below. Regarding the positioning of debris impact, the horizontal position of the point of impact has been randomized for each simulation and each wall (the vertical position depends on the flooding height, assuming floating debris). The values reported in Table 2 have been set by assuming waterborne debris such as rubble or tree trunk. The minimum and maximum values of 0.5 second and 1.5 second, respectively, for the (uniform) distribution of debris impact time are set in order to consider a certain variability respect to the central value of 1.0 second proposed by Autority of Pò River Basin in [49].

Loading parameter	Distribution type	Min	Max	COV [%]
Debris mass (kg)	Uniform	200	500	24.74
Debris impact time (s)	Uniform	0.5	1.5	28.87

Table 2: Continuous uncertain parameters related to loading parameters

2.4 Calculating the critical flood height h(Y=1) for a given realization of vector Θ

As it was mentioned in the previous section, the critical flood height for a given realization of vector θ can be calculated from the IFHA curve as the flood height value that corresponds to Y=1. The systemic variable Y was defined as the critical demand to capacity ratio throughout the structure, defined according to a *"weakest-link"* concept. In other words, Y is calculated as the largest demand to capacity ratio throughout all the walls. Within each wall, zones of high stress concentration can be identified due to, debris impact, asymmetric boundary conditions, and geometrical configurations/presence of openings. Herein, the Y value for each given wall is calculated as the largest demand to capacity ratio for all the critical sections controlled. Figure 7 below shows the critical sections considered for the case-study structure.

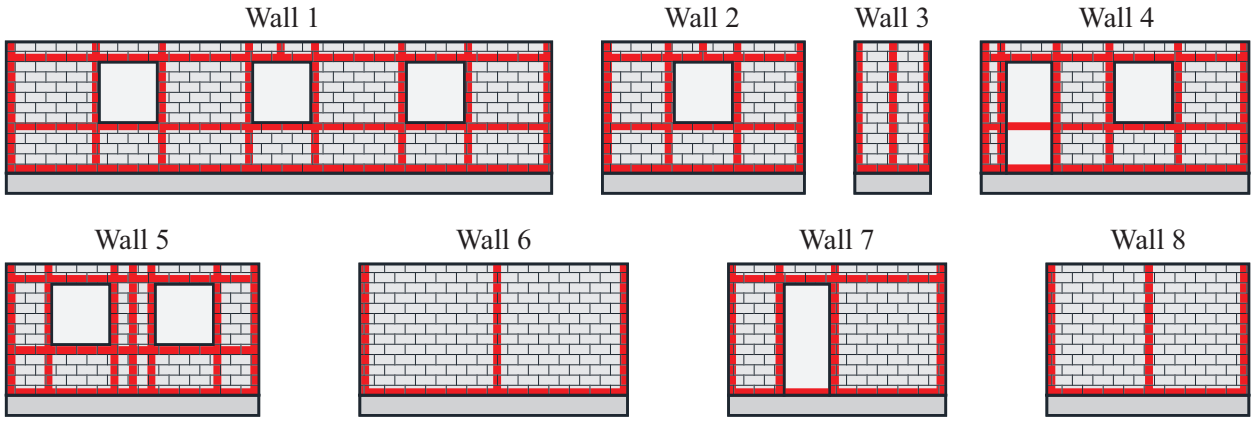

Figure 7: The critical sections considered throughout the case-study structure (highlighted in red color).

For each section examined, a critical demand to capacity ratio is calculated through an iterative procedure. This iterative procedures searches various pieces of the critical section (constructed as integer multipliers of the shell element *"building block"*) in order to find the sub-section with highest stress concentration. This iterative procedure is demonstrated schematically in Figure 8 below for the base section in a wall panel consisted of two windows.

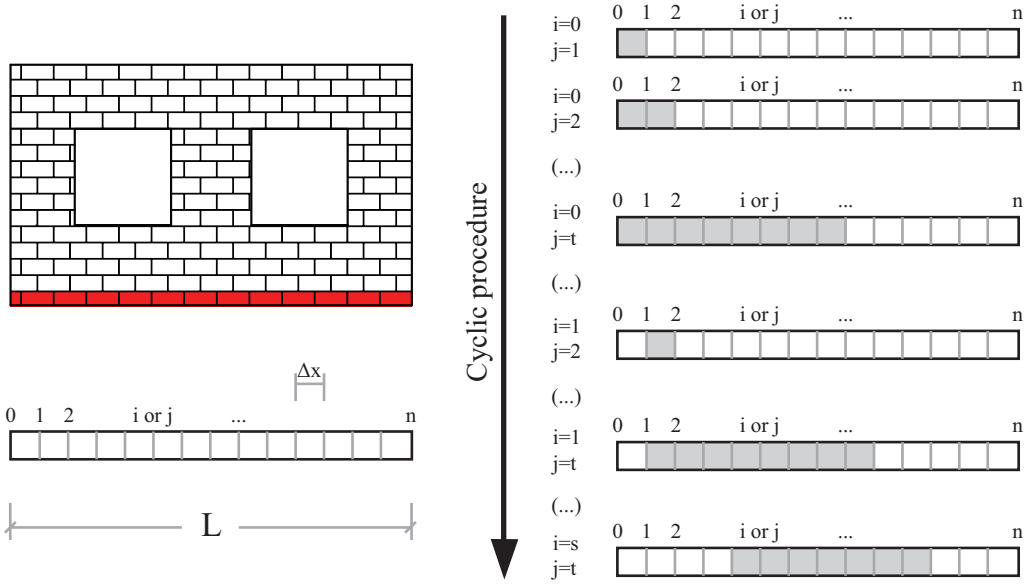

Figure 8: Schematic diagram of the iterative procedure employed in order to identify the zone with highest stress concentration within a given wall section.

For a given a given realization of the vector of the uncertain parameters $\boldsymbol{\Theta}$, the critical demand to capacity ratio (Y, explained in the section 1.2) is calculated as the largest demand to capacity ratio considering both the shear stress and the out-of-plane bending moment. Therefore, for the specific case, Y is equal to:

$$Y = \left(\frac{D}{C}\right)_{Weakest-link} \qquad \text{Eq. 21}$$

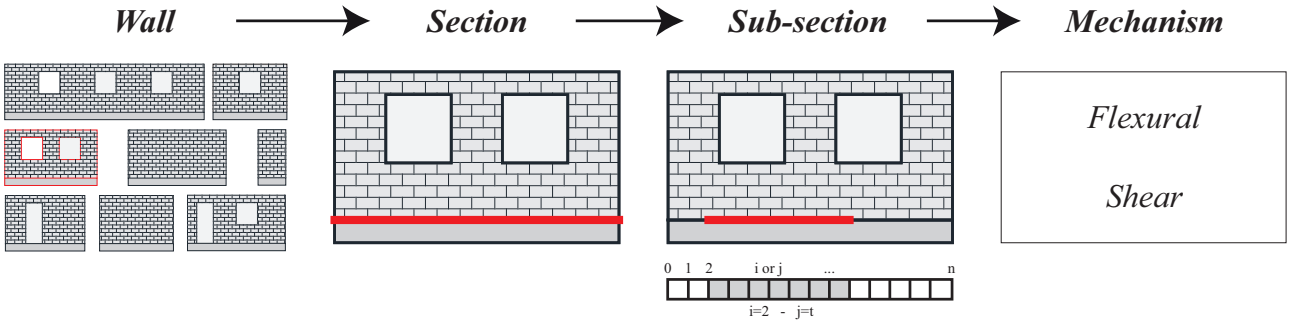

Figure 9: Hierarchy for the identification of weakest-link.

There are several methodologies available in the literature for analyzing the masonry structures subjected to a combination of gravity and lateral loading (mostly for seismic loading). For example, the masonry structures can be analyzed by using the equivalent frame method [50]. Alternatively, the virtual work principle based on a limit analysis approach [51] can be used in order to calculate the loads that can bring the structure (or a part of it) to the verge of instability. On the other hand, several models have been proposed for evaluating the in-plane capacity of masonry walls [52], [53]. Few works so far have dealt with the structural effects of hydrogeological hazards; for example, [54], [39], [55]. The aim of the authors herein is to demonstrate how simple models can be used for evaluation of the vulnerability of non-engineered constructions. This choice is backed by the fact that it can be quite complicated (due to various reasons such as lack of laboratory instrumentation, economic resources, …, etc.) to obtain extensive laboratory and in-situ tests, necessary for detailed modeling, for this specific kind of buildings. Therefore, the aim has been to implement simple models with few parameters that can often be characterized also based on available literature and visual/in-situ testing.

Two different kind of actions are verified herein: 1) out-of-plane bending moments in both horizontal and vertical cross sections; 2) out-of-plane shear stress.

The flexural moment resistance $(M_{Rd,H})$ in horizontal sections is calculated according to [56]:

$$M_{Rd,H} = \frac{N \cdot t}{2} \cdot \left(1 - \frac{N}{0.85 \cdot f_m \cdot A_{section}}\right) \quad \text{Eq. 22}$$

The bending moment capacity is evaluated considering that the out-of-plane bending moment capacity is differentiated with respect to horizontal and vertical sections, due to the (more significant) presence of axial forces. The vertical moment resistance ($M_{Rd,V}$) is evaluated according to Griffith and Vaculik [57].

$$M_{Rd,V} = \frac{f_{fl} \cdot H_{section} \cdot t^2}{6} \quad \text{Eq. 23}$$

The shear strength (V_{Rd}) considering the tangential stress capacity according to Nigro and Faella [21] and CEN [58]:

$$V_{Rd} = A_{section} \cdot \tau_0 \quad \text{Eq. 24}$$

In previous equations: $A_{section}$ is the area of the section/sub-section; τ_0 is the tangential stress capacity; t is the thickness of the wall; f_m is the compression resistance of the masonry along the horizontal sections; f_{fl} is the compression resistance of the masonry along the vertical sections; $H_{section}$ is the height of the section/sub-section; N is the axial force acting on the section/sub-section. The formula for shear strength neglects interactions between shear/axial forces. The flexural strength for a horizontal section/sub-section in **Error! Reference source not found.** assumes that the bending moment strength is reached by means of exceeding the ultimate compression strength. It is worth mentioning that local stress concentrations do not necessarily translate into global failure

mechanisms; however – in lieu of more accurate information – they can be considered as precursors to failure for a brittle structure.

2.5 Incremental analysis curve and demand to capacity ratio graphs

The incremental flood height analysis procedure, which is performed for 20 realizations of the vector of the uncertain parameters, provides the critical (weakest link) demand to capacity ratio Y corresponding to each hydraulic load step, over all the considered mechanisms/sub-sections/sections/walls (see Figure 9 for the heierarchy of the links). Figure 10 below reports the incremental flood height analysis curves for the simulation realizations performed for the case study building.

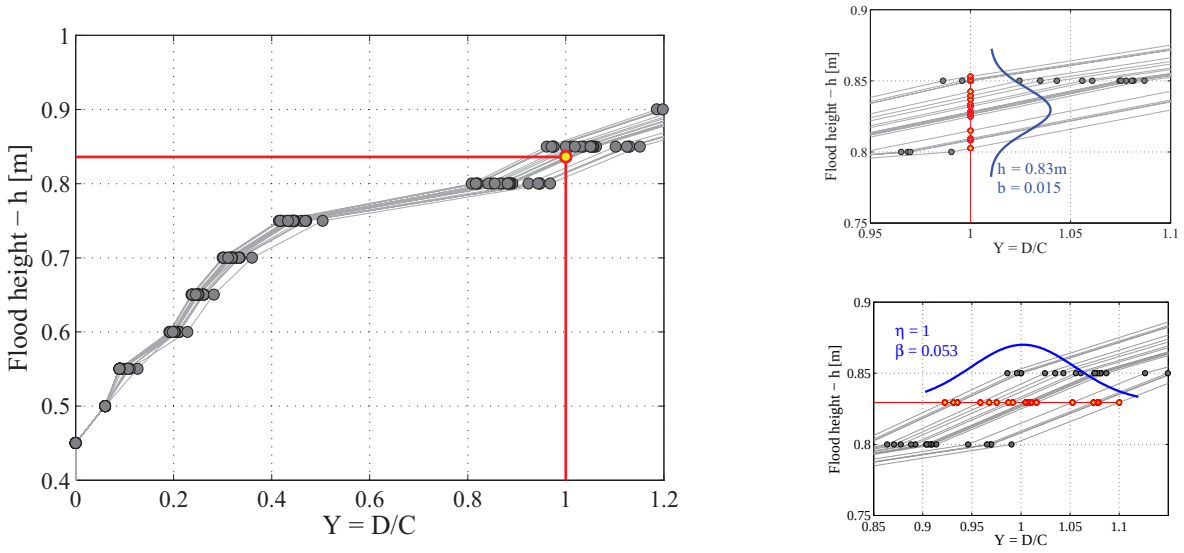

Figure 10: Incremental Flood Height Analysis curves and the lognormal distribution fitted to the sample of critical water height values.

As explained before, the critical water height for each simulation realization is estimated as the flooding height corresponding to Y=1 from the IFHA curve. The median η and the logarithmic standard deviation β for the critical water height can also be evaluated based on the IFHA results. It can be seen that for the case-study structure considered, the critical flood heigh is not very sensitive to the uncertainties in loading and mechanical material properties. It should be noted that the collapse limit state is almost exclusively governed by flexural failure in the horizontal section in the base. The flexural strength in (Eq. 22) in its turn depends strongly on the axial load, thereby on the self weight of the structure. Therefore, the small variability in the critical height values can also be attributed to the relatively small variability in the specific weight (Table 1). The other factor that contributes to the small variability in the critical height values is that the moment in the base has a dimensional relationship of length to the power of three with flooding height. In other words, the variability in the critical demand to capacity ratio for a given flood height (i.e., a horizontal cut through the IFHA curves in Fig. (10)) is much larger than the variability in the critical flood height for Y=1 (a vertical section through the IFHA curves in Fig. (10)). It is worth mentioning that for this specific case study, considering the debris impact does not seem to affect the critical water height significantly.

Figure 11 below depicts in a visual manner how the demand to capacity ratio is calculated and reported for various sub-sections in the lower end of the wall for h=0.80m (by applying Eq. 22, Eq. 23 and Eq. 24 through the procedure illustrated in Figure 8).

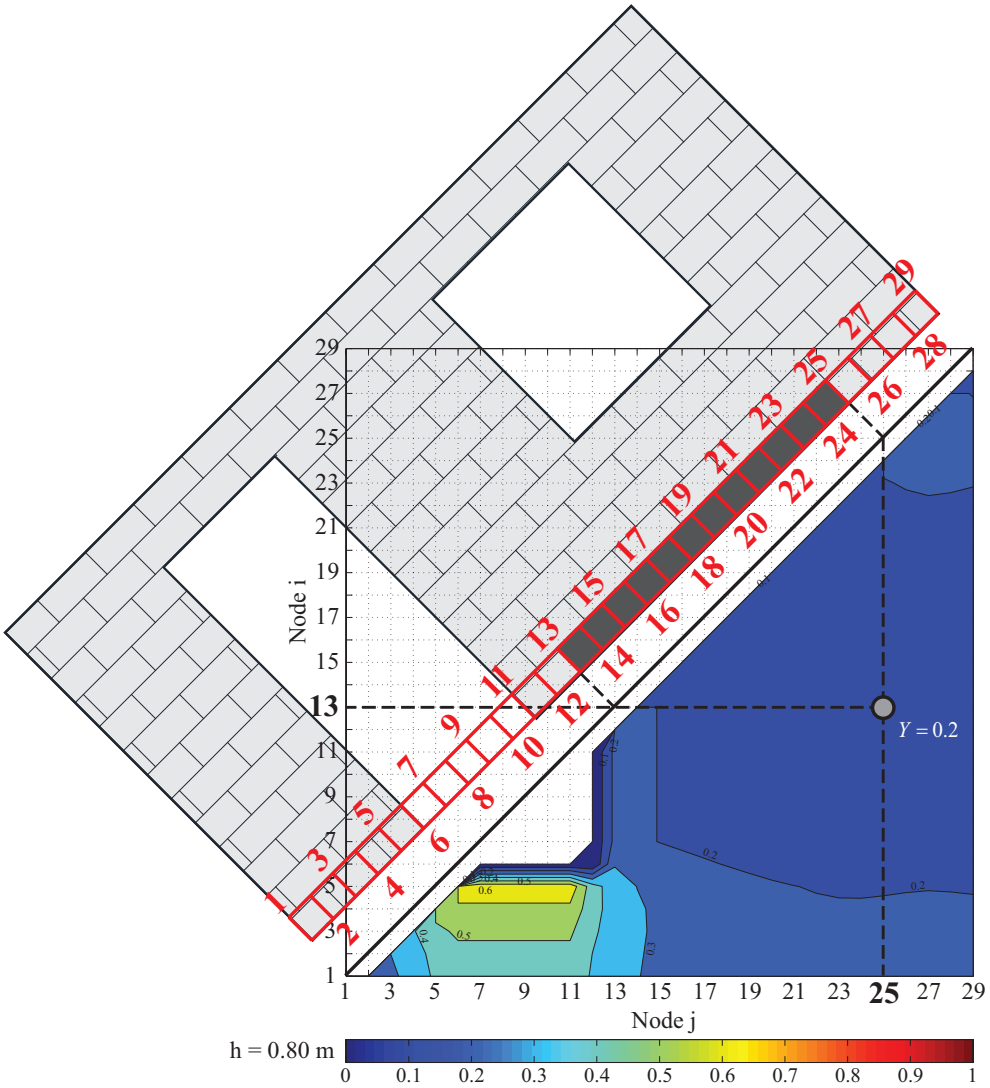

Figure 11: Schematic procedure for identifying the Y value for a sub-section defined by the indexes i and j.

As it can be seen in the figure, each Y value in the contour is associated to a sub-section identified by its beginning and end nodes i and j compatibile with the schematic diagram in Figure 8. It can be observed that these contour diagrams provide efficient and visual means of screening the most critical zones of stress concentration in a given section of a given wall subjected to a specific flooding height. The diagram can also be read in the opposite manner by choosing a specific sub-setcion, identified by its end nodes, and finding the corresponding Y value. For example for the section depicted in Figure 11, the most critical subsections are in the vicinity of the door (to the left) with a Y value of around 0.50.

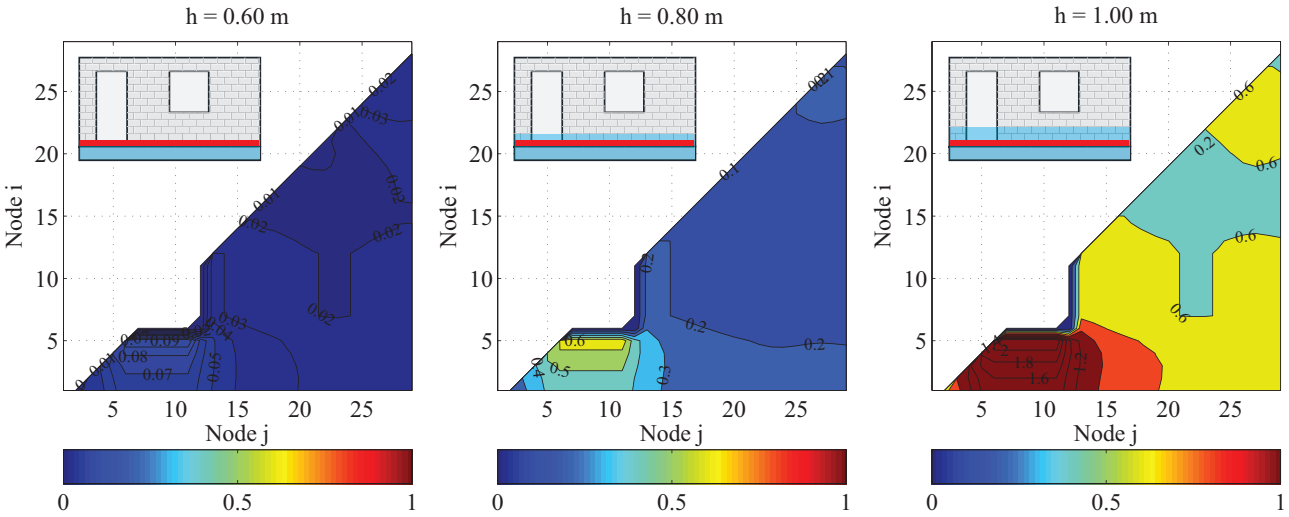

Figure 12: Y values for flexural base mechanism of Wall 4.

Figure 12 reports the demand to capacity ratios (Y values) for flexural mechanism at base for the load steps 0.60, 0.80 and 1.00 meters. As it can be seen, critical sub-sections can be identified for the zone between the door and the extreme lateral section in the left. In a similar manner, Figure 13 illustrates the Y values for the flexural mechanism in the section passing right under the window at the load steps 0.60, 1.00 and 1.20 meters. It can be seen that the critical sub-sections are concentrated in the zone between the door and the extreme left side of the wall. Figure 14 shows the Y values in terms of shear for the vertical section at the side of the door. It can be observed that the zones of high stress are concentrated in proximity of the wall base where a fixed connection is assumed.

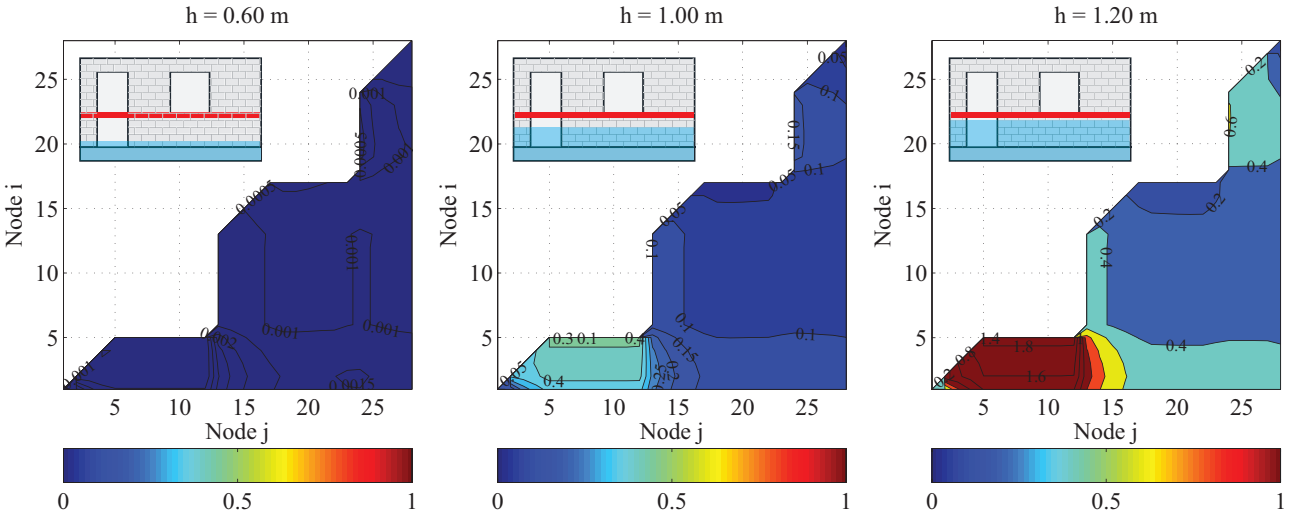

Figure 13: Y values for flexural mechanism under the window for Wall 4.

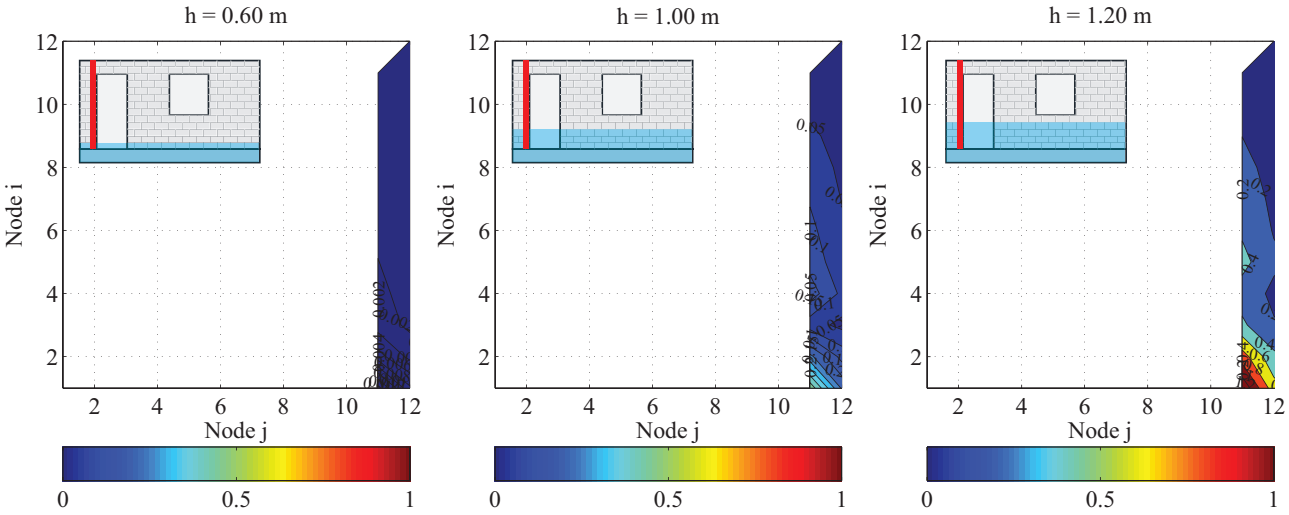

Figure 14: Y values for shear mechanism for the section running alongside the door for Wall 4.

2.6 Performance-based safety-checking

Figure 15 below illustrates the fragility curves calculated for the case-study building for the default condition. The left-hand figure depicts both the fragility curves for the individual walls and the fragility curve for the building as a whole through the weakest-link concept (the thick red line). The right-hand figure depicts the robust fragility curve for the entire building with the plus/minus one standard deviation confidence interval. This confidence interval represents the epistemic uncertainty in the estimation of the robust fragility. The width of the confidence interval is going to decrease as the number of simulations increases. The building failure mode seems to be entirely governed by the flexural failure of the base section in wall number 4 (the same wall that was analyzed in more detail in the previous section) and there is no shift of failure mechanism due to the consideration of uncertainties.

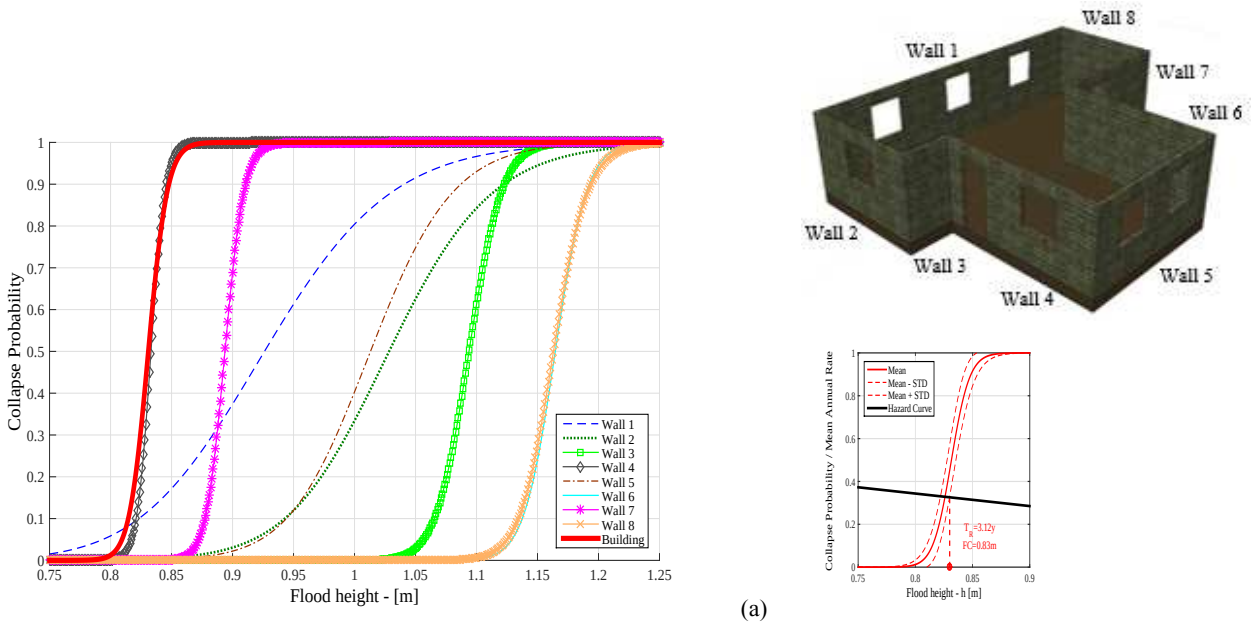

Figure 15: (a) Fragility curves for the individual walls within the default structure (D); (b) the robust fragility curve for the entire structure with the plus/minus one standard deviation confidence interval

2.7 Using the DCFD safety-checking for flood resistance upgrading decision-making

The DCFD safety-checking format can also be used for screening of various viable upgrading strategies for improving the flood resisting characteristics of the case-study building. In this section, some viable upgrading strategies are presented and the corresponding model is assessed using the DCFD format. It should be noted that the proposed solutions are all relatively low-cost and some of them are already implemented by the inhabitants of the zone as viable climate adaptation strategies (in particular, raising the platform). Figure 16 below reports the robust fragility curves for the case study building in default conditions (model D, purple) and also with four viable mitigation strategies:

1. Increasing the platform height from 40cm to 80 cm (model A, green);
2. Upgrading the vertical connection between the walls from hinged to clamped (model B, orange);
3. Filling the door in Wall 4 (model C, dark blue);
4. Filling the doors in Wall 4 and 7 end realizing a door instead of the middle window in Wall 1 (model E, dark green).

For each structural model discussed above, the factored capacity is calculated from Eq. 16. Moreover, the flood hazard curve in terms of the mean annual frequency of exceeding a given flooding height for the site of the building is also plotted (in black solid lines) in the figure. It should be reminded that the inverse of the mean annual frequency of exceeding a given flooding height is equal to the return period of the flooding event. Therefore, the intersection of the flood hazard curve with the vertical dashed lines, representing the factored capacity for each viable model, represents the most extreme flooding event (identified by its return period) that the structure can withstand for the limit state of collapse, according to the DCFD safety-checking format. For each model studied, the flooding risk represented by the mean annual frequency of collapse calculated from Eq. 11 is also reported. Below, each viable upgrading strategy and its effect on the overall flood resisting performance of the building is discussed. Table 3 summarizes the findings in Figure 16 by tabulating the median $\eta_{hY=1}$ and logarithmic standard deviation $\beta_{hY=1}$ for the fragility curves, the logarithmic standard deviation β_U representing the width of the confidence interval (the uncertainty in the parameters of the fragility), the factored capacity FC from Eq. 15, and the factored capacity FC_U taking into account the effect of the epistemic uncertainties.

Increasing platform height (model A, green). This strategy consists in increasing the level of the floor inside the building to reduce the flood water pressure on the walls. It should be emphasized that the raised platform should have sufficient rigidity for resisting the flood uplift pressure and scouring effects. In Figure 16 it can be seen that this strategy leads to a significant reduction in risk (from 29% to 12% approximately) and an increase of around 0.37 meters in the critical flood height capacity corresponding the collapse limit state. The fragility curve for the building with the increased platform height not only reveals a net shift (approximately equal to the increase in platform height) towards higher flood depth values but also seems to have a lower dispersion. In order to explain this, one can recall that the variance in the critical water height depends on the variance in the resisting forces/moments in the critical sections examined (through performance variable Y). In this particular case, the critical section seems to be the section in the base (to the left-hand side of the door) for Wall 4. The variance in the overturning moment in the base is going to be directly related to the water height (through axial force N that depends on the flow density and height in Eq. 22). In case A (increasing the platform height), the flow depth above the platform is going to be smaller that of the case D (lower platform height). This describes the reduction in dispersion in case A with respect to the default case (case D).

Upgrading vertical connection (model B, orange). In order to ensure the presence of a fixed-end connection, special detailing techniques should be employed; such as, use of reinforcement, or special placing of bricks in wall corners. Upgrading of vertical connections may ensure the presence of box effect in the structure and a 3D model would be much more suitable for representing the overall performance of the structure. However, herein, the walls are analyzed individually and the effect of the upgraded connections is not very pronounced. It can be observed that the factored capacity FC is increased from 0.84m to 0.85m and the factored capacity FC_U taking into account the effect of epistemic uncertainties is increased from 0.83m to 0.84. Moreover, no significant decrease is observed in the flooding risk (which is equal to 28%). In other words, merely considering the change in the vertical boundary condition (as it is done herein) indicates a slight change in the global resistance because the base sections (critical sections for this building) are less solicitated compared to the default model D (due to the bending moment developed in the lateral fixed joints in the upgraded case). Nevertheless, the degree to which the vertical boundary conditions are going to affect the overall performance of the building also depends on the building configuration and geometry (e.g., the thickness of the wall, position and number of the openings and the aspect ratio of the walls).

Filling door Wall 4 (model C, dark blue). This is a simple solution to solving the problem of stress concentration in the horizontal base section between the door and the side of the Wall 4. It consists in the closure of the door with cement blocks, using material similar (in terms of mechanical properties) to the blocks of the building. This solution is possible because the building has already another entrance from Wall 7. It can be observed that this solution leads to a small increase in factored critical water height capacity (from 0.83m to 0.88m) and a small decrease in risk (29% to 27%).

Reorganization of openings (model E, dark green). This solution consists in the filling of the existing doors in walls 4 and 7 (since they make the wall mechanical behavior irregular, creating a concentration of stress in the horizontal base section between the doors and the side of the wall) and creating a new door replacing the central window in Wall 1. It can be observed that this solution leads to an increase in factored critical water height capacity from 0.83m to 0.96m and a reduction in flooding risk from 29% to 23%. After the reorganization of doors in the building, Wall 4 is clearly no longer the weakest link. As it can also be observed in Figure 16, in the form of an increase in the dispersion of the corresponding fragility curve (case E, dark green), in this case the weakest link may change for different simulations. That is, considering the uncertainties in the structural and loading modelling parameters can change the governing failure mechanism. However, the overturning moment (horizontal bending in Eq. 22) in the base section of Wall 1 seems to be the predominant failure mode.

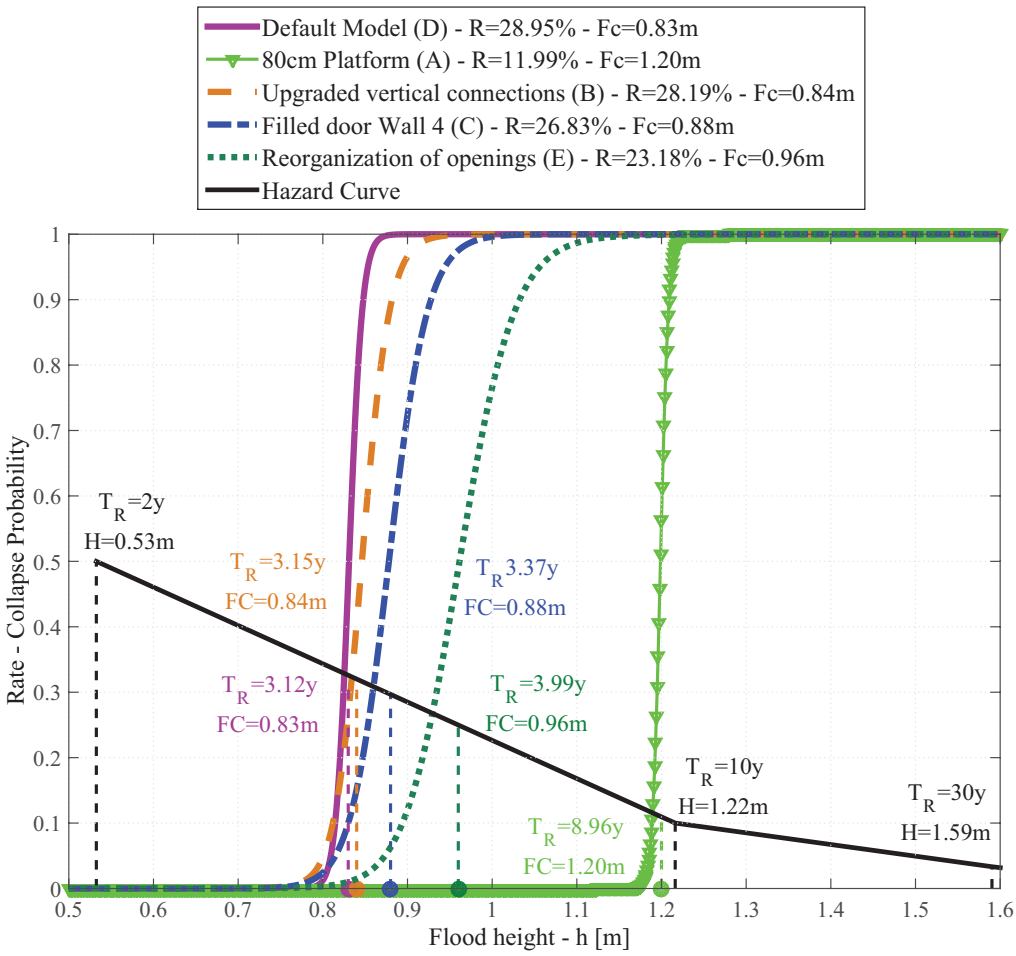

Figure 16: Fragility curves of the building for four different risk mitigation solutions.

Model	$\eta_{h^{Y=1}}$	$\beta_{h^{Y=1}}$	β_U	FC	FC_U	$Risk$	T_R
(D)	0.84 m	1.52 %	0.42 %	0.83 m	0.83 m	28.95 %	3.12 y
(A)	1.20 m	0.66 %	0.17 %	1.20 m	1.20 m	11.99 %	8.96 y
(B)	0.85 m	3.09 %	0.82 %	0.84 m	0.84 m	28.19 %	3.15 y
(C)	0.90 m	4.33 %	1.22 %	0.88 m	0.88 m	26.83 %	3.37 y
(E)	0.98 m	5.44 %	1.55 %	0.96 m	0.96 m	23.18 %	3.99 y

Table 3: Synthesis of the results.

To highlight the stress reduction in Wall 4 produced by the reorganization of openings in the building, the demand to capacity ratio for flexural mechanism in the base section, flexural mechanism under the windows and the shear mechanism at the door side are reported in Figure 17 for a water level of 1.00m. Comparing Figure 17 with the graphs reported in Figure 12, Figure 13 and Figure 14 it is possible to see the benefits induced by the elimination of the door in Wall 4.

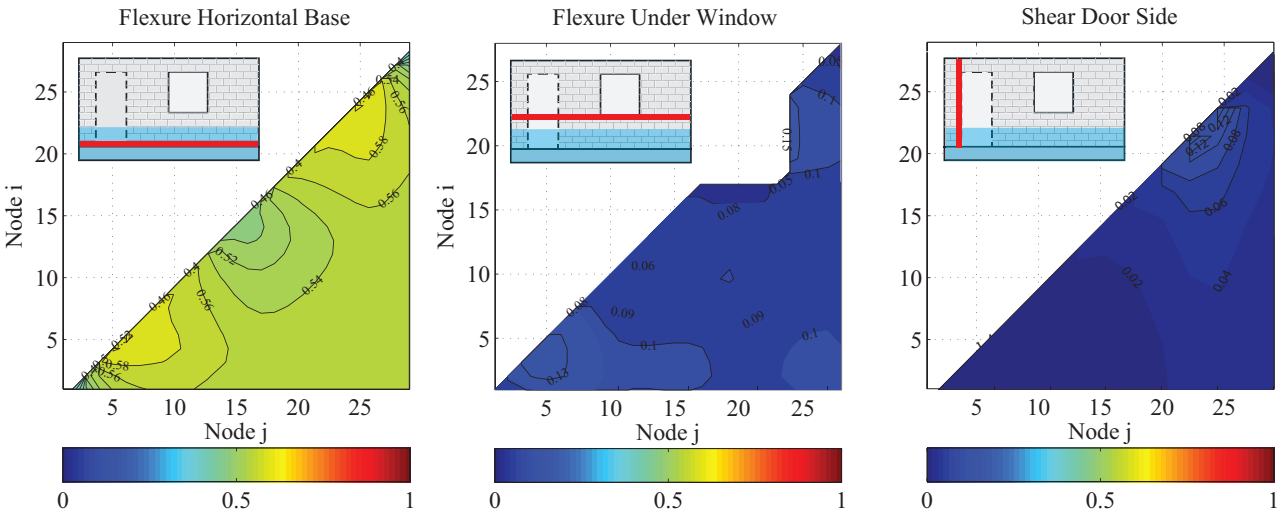

Figure 17: Y ratios for three different sections/mechanisms of Wall 4 in case of reorganization of openings (h = 1.00m).

Conclusive remarks

The probability- and performance-based Demand and Capacity Factor Design (DCFD) format is adopted for flood safety-checking and screening of viable flood resistance upgrading strategies for a case-study informal building located in Suna, Dar Es Salaam. The building is modeled taking into account a compiled visual in-situ survey form. In the absence of specific reinforcement and detailing in corners, it is presumed that the box effect is not going to be present and each wall within the building is modeled separately (using elastic 2D finite element models). Focusing on the collapse limit state, it is assumed that the building is going to reveal a fragile behavior and therefore the assessment is done on the basis of checking allowable stresses within critical sections. The global performance of the building is measured in terms of a critical demand to capacity ratio calculated based on a weakest link philosophy as the demand to capacity ratio for weakest portion of the weakest wall within the structure. An analysis procedure dubbed as the incremental flood height analysis is used in order to find the critical flooding height that corresponds to the onset of unit demand to capacity ratio. The structural fragility is calculated taking into account the uncertainties in loading and material properties and by using an efficient Bayesian procedure providing a robust fragility curve and its plus minus one standard deviation confidence interval. The factored capacity measured in terms of the critical flooding height for the structure can be calculated based on the DCFD formulation taking into account both the logarithmic standard deviation in the fragility curve and also the epistemic uncertainties. The factored demand is calculated as the flooding height corresponding to an acceptable mean annual rate of exceedance, established a priori as a performance objective. A visual representation of the DCFD safety-checking format seems particularly useful as it can depict both the critical water height capacity for the building and also its capacity in terms of the flooding return period it can resist without collapsing. This graphical presentation is useful also for a risk-based screening of various viable upgrading strategies.

With regard to the case-study building, an iterative procedure is used for individuating the stress concentrations in various critical sections in the walls. This is done with the specific objective of finding the critical weakest link demand to capacity ratio for the entire structure, neglecting the box effect. The results are post-processed in order to provide demand to capacity ratio contours for a given section for a given flood height. These plots are quite useful in providing an insight into stress concentrations within various sections. It can be observed that the sources of uncertainties considered do not have a significant effect on the overall performance of the structure. Arguably,

this is because the overall building behavior seems to be invariably governed by a specific section (base section) within a specific wall. In other words, taking into account the uncertainties is not shifting the dominant failure modes. Using the DCFD format for screening of four viable upgrading strategies, it can be observed that raising the foundation of the building is going to significantly improve the overall flood resistance of the building. Moreover, re-organizing the position of the openings in the walls with the aim of creating a more symmetric and regular distribution of openings, is going to lead to a discrete improvement in the flood resisting capacity of the structure (around 10-20% decrease in risk). In general, for the non-engineered structure considered (assuming a fragile behavior due to excessive stress concentrations), the configuration of the walls and the openings is expected to play a significant role in the overall performance of the building.

It should be mentioned that the flooding risk in this work has been calculated by considering the flow depth as the only intensity measure. However, and in order to take into account also the hydrodynamic forces exerted by the flow, it has been assumed that the flow depth and velocity maxima are related through a power-law relation. This assumption, in the context of this work, has the following limiting implications: 1) the maxima in flow depth and velocity are synchronized; 2) the flow velocity maxima in profile occurs at the flow surface level; 3) the hydrodynamic force is orthogonal to the wall.

Clearly, the application of the DCFD format for safety-checking and upgrade decision-making goes beyond the case-study of non-engineered buildings. Moreover, the tools created are also going to be very useful for estimating portfolio fragility curves for a class of buildings as done in [42].

Acknowledgments

This work was supported in part by the European Commission's seventh framework program Climate Change and Urban Vulnerability in Africa (CLUVA), FP7-ENV-2010, Grant No. 265137. The authors would like to gratefully acknowledge Dr. Francesco De Paola for modelling and propagation of riverine flooding for the neighborhood of Suna, Dar Es Salaam. The authors would also like to acknowledge the three anonymous reviewers who have substantially contributed to enriching this work with their insightful comments.

Appendix

GPS COORDINATES	See bottom of page for details			
No. of stories	1		**Height of storey**	2.60m *(up to ceiling level)*
Presence of mezzanine (mansard)			Yes:	No: ✓
Geometric size				
L (plan length)	9.030m		W (plan width)	10.80m
Wall material	Cement blocks			
Wall thickness	0.125m			
Presence of cross connection in the corners			Yes: ✓	No:
Presence of buttress			Yes:	No: ✓
Presence of plaster			Yes: - *half wall, about 1.10m of glazed plaster, at front elevation*	No: ✓
Presence of water-proof paint			Yes:	No:
If wall material is wood and mud	Are wooden piles anchored in foundations?		Yes:	No:
	Are the wooden horizontal piles connected and continuous over the perimeter?		Yes:	No:
Roof typology	Flat:		Pitch:	One side:
				Two side: ✓
	Structural material (a)		Corrugated Iron Sheets	
	Presence of roof beams		Yes: ✓	If yes, material (b): *Wood/Softwood timber, untreated*
			No:	
	Presence of drainage or drip		Yes:	No: ✓
	Presence of roof coverage		Yes: ✓	If yes, material (c): *Corrugated Iron Sheets, Gauge 30*
			No:	
	Use of water proof materials		Yes:	If yes, material:
			No: ✓	
Presence of foundation	No:	Yes: ✓	If Yes:	
			Construction material:	• Plain concrete
			Elevation from ground:	
Presence of lintel beam	*-half beam (over doors and windows)*		Yes: ✓ (200mm thick)	No:
Functionality of doors and windows (in impeding/delaying the water entrance)	Quality of doors:		Good:	Bad: ✓
	Quality of the windows:		Good:	Bad: ✓
Minimum height of the window above the floor	1.15m			
Window dimensions	**L (plan length)**	1.15	**H (height)**	1.20
Height of the door above the floor	** 0.40m			
Door dimensions	**L (plan length)**	0.90	**H (height)**	2.15
Presence of barrier in front of the door	Yes: ✓	No:	If Yes: Elevation from ground	0.40m

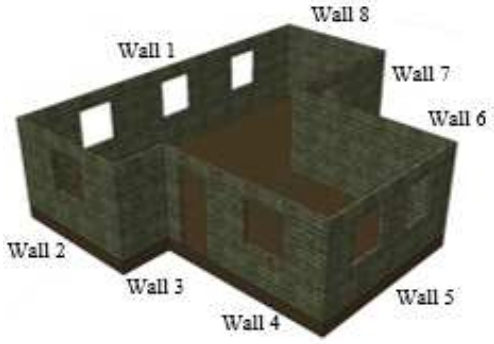

References

[1] Smith DI, Greenaway MA. The computer assessment of urban flood damage: ANUFLOOD. Newton, R W, Sharpe, R, and Taylor, MA R (eds), Desktop Planning, Advanced Microcomputer Applications for Physical and Social Infrastructure Planning, Hargreen, Melbourne. 1988:239-50.
[2] Torres MA, Jaimes MA, Reinoso E, Ordaz M. Event-based approach for probabilistic flood risk assessment. International Journal of River Basin Management. 2013:1-13.
[3] Davis SA. Business Depth-Damage Analysis Procedures. DTIC Document; 1985.
[4] Scawthorn C, Blais N, Seligson H, Tate E, Mifflin E, Thomas W et al. HAZUS-MH flood loss estimation methodology. I: Overview and flood hazard characterization. Natural Hazards Review. 2006;7:60-71.
[5] Scawthorn C, Flores P, Blais N, Seligson H, Tate E, Chang S et al. HAZUS-MH flood loss estimation methodology. II. Damage and loss assessment. Natural Hazards Review. 2006;7:72-81.
[6] Jonkman SN, Vrijling JK, Vrouwenvelder ACWM. Methods for the estimation of loss of life due to floods: a literature review and a proposal for a new method. Natural Hazards. 2008;46:353-89.
[7] Tapsell SM, Penning-Rowsell EC, Tunstall SM, Wilson TL. Vulnerability to flooding: health and social dimensions. Philos T Roy Soc A. 2002;360:1511-25.
[8] Pistrika A, Tsakiris G. Flood risk assessment: A methodological framework. Water Resources Management: New Approaches and Technologies European Water Resources Association, Chania, Crete-Greece2007.
[9] Pistrika A. Flood Damage Estimation based on Flood Simulation Scenarios and a GIS Platform. EWRA 7th International Conference "Water Resources Conservancy and Risk Reduction Under Climatic Instability". Limassol, Cyprus2009. p. 419-27.
[10] Smith D. Flood damage estimation- A review of urban stage-damage curves and loss functions. Water S A. 1994;20:231-8.
[11] Schwarz J, Maiwald H. Damage and loss prediction model based on the vulnerability of building types. 4th International symposium of Flood Defence. Toronto, Canada2008.
[12] Bouchard B. Improving flood risk management in informal settlements of Cape Town. 2007.
[13] Kelman I. Ph.D Thesis: Physical flood vulnerability of residential properties in coastal, eastern England: University of Cambridge; 2002.
[14] Groenevelt PH, Grunthal PE. Utilisation of crumb rubber as a soil amendment for sports turf. Soil Till Res. 1998;47:169-72.
[15] Schwarz J, Maiwald H. Empirical vulnerability assessment and damage for description natural hazards following the principles of modern macroseismic scales. 14th WCEE - World Conference of Earthquake Engineering. Lisboa, Portugal2012.
[16] Charvet I, Ioannou I, Rossetto T, Suppasri A, Imamura F. Empirical fragility assessment of buildings affected by the 2011 Great East Japan tsunami using improved statistical models. Natural Hazards. 2014:1-23.
[17] Haugen ED, Kaynia AM. Vulnerability of structures impacted by debris flow. Landslides and Engineered Slopes: From the Past to the Future, Vols 1 and 2. 2008:381-7.
[18] Nadal NC, Zapata RE, Pagán I, López R, Agudelo J. Building damage due to riverine and coastal floods. Journal of Water Resources Planning and Management. 2009;136:327-36.
[19] Dawson R, Hall J, Sayers P, Bates P, Rosu C. Sampling-based flood risk analysis for fluvial dike systems. Stochastic Environmental Research and Risk Assessment. 2005;19:388-402.
[20] Yue L, Ellingwood BR. Hurricane damage to residential construction in the US: Importance of uncertainty modeling in risk assessment. Engineering Structures. 2006;28:1009-18.
[21] Nigro E, Faella C. Landslides as a secondary event of earthquakes and eruptions. Urban Habitat Constructions Under Catastrophic Events: Proceedings of the COST C26 Action Final Conference: CRC Press; 2010. p. 153.

[22] De Risi R, Jalayer F, de Paola F, Iervolino I, Giugni M, Topa ME et al. Flood risk assessment for informal settlements. Natural Hazards. 2013;69:1003-32.
[23] Jalayer F, De Risi R, De Paola F, Giugni M, Manfredi G, Gasparini P et al. Probabilistic GIS-based method for delineation of urban flooding risk hotspots. Natural Hazards - under review. 2013.
[24] Jalayer F, De Risi R, Kyessi A, Mbuya E, Yonas N. Vulnerability of Built Environment to Flooding in African Cities. Urban Vulnerability and Climate Change in Africa: Springer; 2015. p. 77-106.
[25] De Risi R, Jalayer F, De Paola F, Giugni M. Probabilistic delineation of flood-prone areas based on a digital elevation model and the extent of historical flooding: the case of Ouagadougou. Boletín geológico y minero. 2014;125:329-40.
[26] De Risi R, Jalayer F, De Paola F. Meso-scale hazard zoning of potentially flood prone areas. Journal of Hydrology. 2015;527:316-25.
[27] Cornell CA, Krawinkler H. Progress and challenges in seismic performance assessment. PEER Center News. 2000;3:1-3.
[28] Cornell CA, Jalayer F, Hamburger RO, Foutch DA. Probabilistic basis for 2000 SAC Federal Emergency Management Agency steel moment frame guidelines. Journal of Structural Engineering. 2002;128:526-33.
[29] Jalayer F, Cornell CA. Alternative non-linear demand estimation methods for probability-based seismic assessments. Earthquake Engineering & Structural Dynamics. 2009;38:951-72.
[30] Carozza S, Jalayer F, De Risi R, Manfredi G, Mbuya E. Comparing alternative flood mitigation strategies for non-engineered masonry structures using Demand and Capacity Factored Design. ICASP12, 12th International Conference on Application of Statistics and Probability in Civil Engineering. Vancouver2015.
[31] Ditlevsen O, Madsen HO. Structural reliability methods: Citeseer; 1996.
[32] Vamvatsikos D, Cornell CA. Applied incremental dynamic analysis. Earthq Spectra. 2004;20:523-53.
[33] Jalayer F, Franchin P, Pinto PE. A scalar damage measure for seismic reliability analysis of RC frames. Earthquake Engineering & Structural Dynamics. 2007;36:2059-79.
[34] Jalayer F, De Risi R, Elefante L, Manfredi G. Robust fragility assessment using Bayesian parameter estimation. In: C. Adam RH, W. Lenhardt & C. Schranz, editor. Vienna Congress on Recent Advances in Earthquake Engineering and Structural Dynamics 2013 (VEESD 2013). Vienna, Austria2013.
[35] Jalayer F, De Risi R, Manfredi G. Bayesian Cloud Analysis: efficient structural fragility assessment using linear regression. Bulletin of Earthquake Engineering. 2015;13:1183-203.
[36] Jaynes ET. Probability theory: the logic of science: Cambridge university press; 2003.
[37] Box GEP, Tiao GC. Bayesian Inference in Statistical Analysis: John Wiley & Sons, Inc; 1992.
[38] Jalayer F, Cornell CA. A technical framework for probability-based demand and capacity factor design (DCFD) seismic formats: Pacific Earthquake Engineering Research Center; 2004.
[39] Kelman I, Spence R. An overview of flood actions on buildings. Engineering Geology. 2004;73:297-309.
[40] Roos W, Waarts P, Vrouwenvelder A. Damage to buildings. Delft Cluster paper. 2003.
[41] FEMA FEMA. Manual Coastal Construction. Washington, D.C., USA: Federal Emergency Management Agency; 2000.
[42] De Risi R, Jalayer F, Iervolino I, Manfredi G, Carozza S. VISK: a GIS-compatible platform for micro-scale assessmen of flooding risk in urban areas. In: Papadrakakis M, Papadopoulos V, Plevris V, editors. COMPDYN, 4th ECCOMAS Thematic Conference on Computational Methods in Structural Dynamics and Earthquake Engineering. Kos Island, Greece2013.
[43] FEMA FEMA. Report 259. Engineering principles and practices for retrofitting floodprone residential buildings. Washington, D.C., USA.1995.
[44] NAASRA NAoASRA. Highway Bridge Design Specification. Sydney, Australia.1990.
[45] AASHTO AAoSHaTO. LRFD Bridge Design Specifications, 2nd edn. American Association of State Highways and Transportation Officials. Washington, DC., USA.1998.

[46] De Risi R, Jalayer F, Iervolino I, Kyessi A, Mbuya E, Yeshitela K et al. D2.4 - Guidelines for vulnerability assessment and reinforcement measures of adobe houses. CLUVA project - Climate Change and Urban Vulnerability in Africa2012.
[47] Carozza S, De Risi R, Jalayer F. D2.5 - Guideline to Decreasing Physical Vulnerability in the Three Considered Cities. CLUVA project - Climate Change and Urban Vulnerability in Africa2013.
[48] McKenna F, Fenves GL, Scott MH. OpenSees: Open system for earthquake engineering simulation. Pacific Earthquake Engineering Center, University of California, Berkeley, CA. 2006.
[49] Basin AoPR. Edifici in aree a rischio di alluvione: come ridurne la vulnerabilità. 2007.
[50] Kappos AJ, Penelis GG, Drakopoulos CG. Evaluation of simplified models for lateral load analysis of unreinforced masonry buildings. Journal of structural Engineering. 2002;128:890-7.
[51] Livesley R. A computational model for the limit analysis of three-dimensional masonry structures. Meccanica. 1992;27:161-72.
[52] Betti M, Galano L, Petracchi M, Vignoli A. Seismic Strength of Unreinforced Masonry Walls: Effects of the b Shape Factor of the Shear Failure Criterion with Diagonal Cracking. 2012.
[53] Anthoine A. Derivation of the in-plane elastic characteristics of masonry through homogenization theory. International Journal of Solids and Structures. 1995;32:137-63.
[54] Faella C, Nigro E. Dynamic impact of the debris flows on the constructions during the hydrogeological disaster in Campania-1998: failure mechanical models and evaluation of the impact velocity. Proceedings of the international conference on FSM, Naples, Italy2003. p. 179-86.
[55] De Risi R, Jalayer F, De Paola F, Iervolino I, Giugni M, Topa M et al. Flood risk assessment for informal settlements. Natural hazards. 2013;69:1003-32.
[56] IBC. Italian Building Code, DM 14.01. 2008: Norme tecniche per le costruzioni. Italian Ministry of Infrastructures and Transportation, Rome. 2008.
[57] Griffith M, Vaculik J. Out-of-plane flexural strength of unreinforced clay brick masonry walls. TMS Journal. 2007;25:53-68.
[58] CEN. Eurocode 6: Design of masonry structures–Part 1–1: Common rules for reinforced and unreinforced masonry structures. ENV 1996-1-1: 2004: E, CEN Brussels; 2004.